Multipath Modeling of Automotive Power Line Communication Channels

Multipath Modeling of Automotive Power Line Communication Channels

Igor S. Stievano, *Senior Member, IEEE,* Flavio G. Canavero, *Fellow, IEEE,* Williams Richard Garcia Valverde, Lorenzo Guerrieri and Paola Bisaglia

***Abstract*—In this paper an in-vehicle power line channel mathematical multipath representation is proposed. The selected approach aims at describing the transmission of a signal on a possibly complex power network by means of a finite number of delayed echoes. Model parameters are computed via a well-defined step-by-step procedure from frequency-domain channel characteristics. The feasibility and strength of the method are demonstrated by means of a measurement campaign. Two-port scattering measurements have been carried out on a commercial automobile and the effect of the measurement setup has been considered in the analysis.**

***Index Terms*—Power distribution, Modeling, Transmission lines, Multipath channels, Automotive, Power line communication.**

I. Introduction

Nowadays modern automobiles include many electronic systems and subsystems for both safety and comfort. Well known examples are control circuits for electronic stability, airbags, sensors spread all over the car as well as audio and visual equipment. According to the Society for Automotive Engineers (SAE), different classes of protocol communications are present in the automotive domain: they go from the low speed Class A (≤ 10 kbit/s) used for exchanging control data in the body domain (an example is lighting control) to the high speed Class D (≥ 1 Mbit/s) for safety-related and multimedia real time communications, including medium speed Class B ($10 - 125$ kbit/s) and Class C ($125 - 1000$ kbit/s) used for communications among the different electronic control units (ECU) in the body domain and in the powertrain and chassis domains, respectively [1]. Complying with these class requirements, at present, the communication in cars is mostly implemented using three common bus protocols: local interconnect network (LIN), controller area network (CAN) and FlexRay. The LIN bus provides time-triggered communication at speeds of 20 kbit/s at 40 meters bus length, the CAN bus reaches bit rates up to 1 Mbit/s with network lengths below 40 meters and the FlexRay meets the higher bandwidth requirements with 10 Mbit/s data rate per channel (two channels are used) in event-triggered communications. All these protocols use the DC line as power supply and dedicated wires to realize the communication [2]. In [3], it is reported that 80% of innovation in a new car is due to electronics, a trend that has certainly continued in recent years thus raising up the number of ECU and confirming the statement in [3] that the single most expensive car component is the wiring harness. The costs associated to wiring are not only limited to the cost of the material and of the modules implementing the just mentioned communication protocols: new wires raise up the weight of the car, thus increasing the gasoline consumption, require a complex design of the interconnection networks to guarantee communication reliability while avoiding cross-interferences and make the diagnostic of a problem more complex [4].

In this framework, a promising solution that helps to reduce the number of wires and the associated costs is represented by power line communication (PLC) technology that has already been successfully implemented in different applications [5], [6], [7], [8], [9], [10], [11], [12], [13], [14]. PLC modems can be used to communicate between two points in the car via the power distribution network, without additional dedicated wires for data exchange. This solution relies on standard circuits and communication schemes, thus making this choice an effective alternative for this class of applications. In particular, in the last decade, substantial progresses have been done in the development of in-home power line communication. For instance, the widespread adopted standard Homeplug AV [15] allows a maximum data rate of 200 Mbit/s and the HomePlug Alliance has recently released the Gbit/s class technology HomePlug AV2 [16]. These numbers are significantly higher than the automotive ones (lower than 10 Mbit/s: note that traditional protocols are trying to compensate this low throughput through information compression techniques [17]), raising the question if the power line technology can be successfully employed in the automotive domain as well. Research should address all the necessary modifications in order to achieve the automotive requirements [4].

Numerical models of the automotive PLC channel are required for assessing strengths and limitations of application designs implementing the PLC technology. Recent literature has proposed contributions with specific emphasis on the characterization of the power line communication channels from real measurements [18], [19]. Also, a number of alternative modeling methodologies have been proposed. Without loss of generality, we limit ourselves to the results on the physical-based modeling of the power delivery network via the cascade

Manuscript received March 8, 2013; revised May 31, 2013 and September 6, 2013; accepted November 21, 2013.

I.S. Stievano and F. G. Canavero are with the Department of Electronics and Telecommunications, Politecnico di Torino, Corso Duca degli Abruzzi, 24, 10129, Torino, Italy, e-mail: {igor.stievano, flavio.canavero}@polito.it.

W. R. Garcia Valverde, L. Guerrieri and P. Bisaglia are with DORA S.p.A., STMicroelectronics group, Via Lavoratori Vittime del Col du Mont 28, 11100 Aosta, Italy, e-mail: {williams-dora-spa.garcia, lorenzo-dora-spa.guerrieri, paola-dora-spa.bisaglia}@st.com.

connection of multiport lumped equivalents, multiconductor transmission lines or digital filters [20], [21], [22], [23], [24], [25]. The above class of approaches, while providing accurate results in reproducing the behavior of real power networks, requires detailed knowledge of the possibly complex interconnected structures (that is hardly available to PLC designers). The length and cross section of wires, as well as the information on materials need to be known. As an alternative, simplified formulas from digital signal processing theory can be used [26]. This method, however, represents an oversimplification of the real channel, with the aim of generating an initial guess for the quantitative computation of the performance of the PLC channel [27]. Of course, the direct use of frequency-domain measurements is always a possible alternative that does not introduce any modeling effort and that is limited to the availability of experimental data. In other words, this approach does not allow designers to rely on a mathematical model whose parameters are representative of the application at hand and that can be effectively used in a possible hardware or software channel emulator [28]. When the power network is considered as a black-box, a purely behavioral approach can be used instead [29]. This approach, which is based on model representations that are suitable to describe the point-to-point behavior of a PLC channel, has several strengths. Mainly, the model structure is defined by a limited number of parameters that can be determined from real measured data, via a well-defined procedure, and the model accuracy and complexity can be easily tuned by setting an appropriate threshold during the model estimation. Preliminary results on the application of the method on a set of freely available measurements have been presented in [30], [31].

The aim of this paper is two-fold: to apply the behavioral modeling approach to the case of PLC in-vehicle channels and to describe the channel measurement campaign done in a commercial automobile (including the measurement setup and data pre-processing). The proposed modeling procedure has been applied systematically to all the available measurements to collect some statistical information on model complexity.

II. Multipath model representation

This section describes the model representation assumed to accurately reproduce the behavior of an arbitrary power distribution network and outlines the procedure for the estimation of model parameters from real measured data. The applicability of the proposed modeling strategy ranges from the traditional power networks found in buildings to the dedicated interconnection of wires supplying energy to industrial equipments or electrical and electronic components in vehicles (cars, ships and airplanes are all covered in this classification). A simplified and ideal power line structure and analytical computations are discussed to justify the proposed black-box model structure and its extension to handle a variety of power networks within the same modeling framework.

A. Scalar power line structure

Regardless of the specific application at hand, a typical power distribution system consists of a complex interconnected structure of multiconductor power lines. For the sake of illustration, our discussion is based on the scheme of Fig. 1. The above example, in the Laplace domain, represents a wire over a ground plane connecting a source on the left (here described by a simple Thevenin equivalent) to a load on the right. The power line channel connecting the source to the load is represented by a scalar transmission line governed by the well-known telegrapher equations [32]. Even if the circuit of Fig. 1 provides a rough simplification of real structures, it offers a representative example of a distributed link and allows to derive clearly and via simple analytical computation the model representation assumed hereafter in the paper.

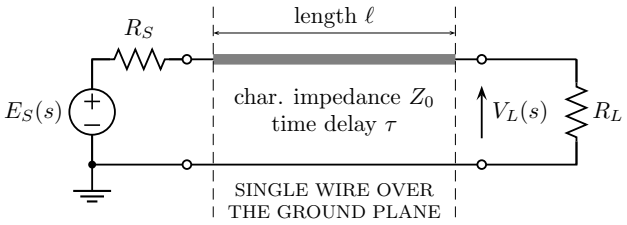

Fig. 1. Equivalent circuit in the Laplace domain providing a simple point-to-point power communication scheme between a transmitter on the left and a receiver on the right. The transmitter is oversimplified by a series Thevenin equivalent and the receiver by a resistor.

The dynamical features of the propagation of the transmitted signal $E_S(s)$ to the right-hand side of the line is taken into account by the network function $H(s) = V_L(s)/E_S(s)$, where $V_L(s)$ is the received voltage. According to [32], the network function $H(s)$ writes:

$$H(s) = \frac{Z_0(1+\Gamma_L)}{R_S+Z_0}\frac{\exp(-s\tau)}{1-\Gamma_S\Gamma_L\exp(-2s\tau)} \quad (1)$$

where Z_0 denotes the characteristic impedance, τ the time delay and Γ_S and Γ_L are the so-called reflection coefficients defined by $\Gamma_S = (R_S - Z_0)/(R_S + Z_0)$ and $\Gamma_L = (R_L - Z_0)/(R_L + Z_0)$, respectively; they are real numbers that account for the effects of the resistors R_S and R_L on the line response.

In order to gain insight on the behavior of the structure of Fig. 1, the network function (1) is expanded in polynomial series, leading to:

$$\begin{aligned} H(s) \cong\ & \frac{Z_0(1+\Gamma_L)}{R_S+Z_0}[\exp(-s\tau)+\Gamma_S\Gamma_L\exp(-3s\tau) \\ & +(\Gamma_S\Gamma_L)^2\exp(-5s\tau) \\ & +(\Gamma_S\Gamma_L)^3\exp(-7s\tau)+\ldots] \end{aligned} \quad (2)$$

The above equation, that holds under the condition that the term $\Gamma_S\Gamma_L\exp(-2s\tau)$ is less than one in magnitude, can be conveniently rewritten as:

$$\begin{aligned} H(s) \cong\ & g_1\exp(-s\tau)+g_2\exp(-3s\tau) \\ & +g_3\exp(-5s\tau)+g_4\exp(-7s\tau)+\ldots. \end{aligned} \quad (3)$$

where g_k are weighting coefficients that depend on the specific structure at hand (e.g. $g_1 = Z_0(1+\Gamma_L)/(R_S+Z_0)$, $g_2 = \Gamma_S\Gamma_L Z_0(1+\Gamma_L)/(R_S+Z_0), \ldots$ for the scheme of Fig. 1).

The number of terms required by the truncated expansion (3) to reproduce the original reference response defined by (1) depends on the desired accuracy and on the maximum frequency band of interest. As an example, Fig. 2 shows the magnitude of the frequency-domain response of the transfer function $H(s)$, i.e. $|H(s{=}j\omega)|$ where $\omega{=}2\pi f$ is the angular frequency. The reference response (solid line) is superimposed by the response of the truncated four-term expansion (3) (dashed line) in the figure. Indeed, a larger number of terms can be considered to increase the accuracy, thus leading to indistinguishable responses. In this comparison, the frequency span has been selected in a range representative of the typical values considered in the experimental characterization of the power line channel for automotive applications.

Equation (3) can be easily converted to the time-domain, with the exponential terms in the Laplace domain $\exp(-ks\tau)$ mapping to the corresponding delayed contributions $\delta(t-k\tau)$. According to this rule, the time-domain *impulse* response $h(t) = \mathcal{L}^{-1}\{H(s)\}$ ($\mathcal{L}^{-1}$ being the inverse Laplace operator) can be used to compute the received transient far-end voltage response $v_L(t)$. This is achieved by means of the convolution between the time-domain transmitted signal $e_S(t)$ and the impulse response $h(t)$, leading to:

$$v_L(t) = h(t) * e_S(t) \cong g_1\, e_S(t-\tau) + g_2\, e_S(t-3\tau) + g_3\, e_S(t-5\tau) + g_4\, e_S(t-7\tau) + \ldots. \quad (4)$$

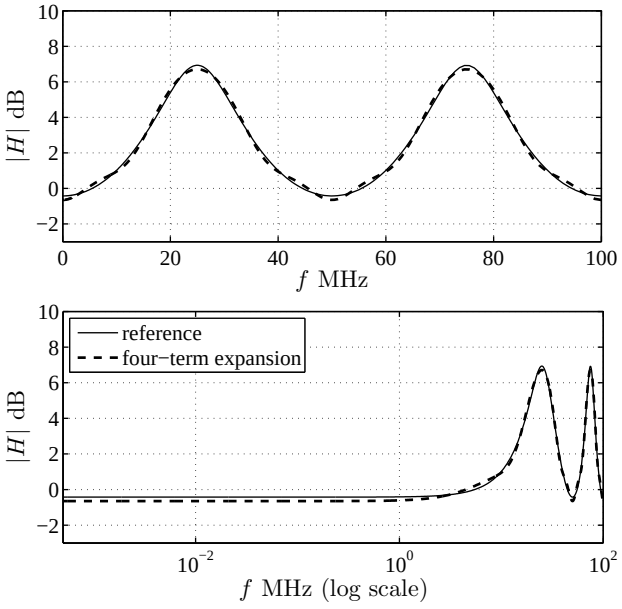

Fig. 2. Magnitude of the $H(j\omega)$ transfer function of the example line of Fig. 1. The parameters defining the structure of Fig. 1 are: $R_S = 10\,\Omega$, $R_L = 200\,\Omega$, line length $\ell = 3\,\text{m}$ (the line is assumed ideal and lossless, defined by a characteristic impedance $Z_0 = 50\,\Omega$ and a propagation delay $\tau = 10\,\text{ns}$). Top panel: linear frequency-axis; bottom panel: same plot with logarithmic frequency-axis. The frequency range [500 Hz , 100 MHz] is chosen to be representative for the application considered in this study, i.e. the characterization of automotive power lines with typical line length of wires on the order of some meters. Solid line: channel response obtained from the analytical equation (1); dashed line: response of the truncated four-term expansion (3).

For a more informative and graphical interpretation of (4), Fig. 3 shows the first four contributions of the series expansion for a transmitted pulsed signal $e_S(t)$ (being the latter also shown in the figure).

The above example clearly illustrates the basic mechanism of the transmission of a signal through a PLC channel: a signal (i.e. a pulse in our example) sent on a distributed interconnection is corrupted by multiple reflections, and this leads to an infinite number of delayed echoes of the transmitted signal reaching the far-end side of the line. The same behavior can be observed and derived for more complex structures consisting of multiple lines with branches (as in the typical power distribution networks). The only difference in this more realistic case is that the delays in (4) are not multiples of the single delay τ and depend on the lengths (i.e. the propagation delays) and characteristics of the different branches composing the structure. Also, the coefficients multiplying the delayed replicas of the transmitted signal will be numbers depending on the topology of the structure and its parameters.

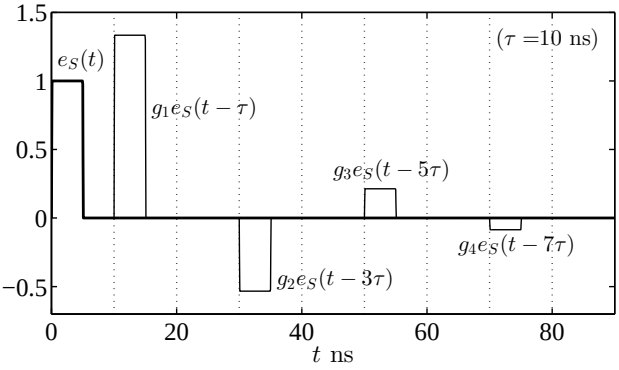

Fig. 3. Example of a time-domain signal $e_S(t)$ sent on the line of Fig. 1 and the corresponding echoes arising from the different delayed terms of (4).

B. Extension to complex interconnected structures

Figure 4 shows a second example representing the interconnected network of four transmission lines. Each segment corresponds to a two-conductor line as the one of Fig. 1 with a characteristic impedance $Z_0 = 50\,\Omega$ and suitable length and propagation delay (being this information shown in the figure). The far-ends of the lines (i.e., the points B, C and D) are terminated with $200\,\Omega$ resistors. A voltage signal is transmitted in A via a Thevenin equivalent with $10\,\Omega$ series resistor and received in D as the voltage across the terminating resistor. The two gray arrows shown in the figure are two example paths $(A \to E \to D)$ and $(A \to B \to A \to E \to D)$ followed by an electrical signal starting from A and reaching point D. The above example is aimed at verifying the behavior of more complex interconnected structures consisting of transmission lines and lumped terminations, thus covering the gap between the tutorial example of Sec. II-A and the real in-vehicle power line structure discussed hereafter in this study.

For this second test case, Fig. 5 shows the time-domain response of the received voltage to a $0.5\,\text{ns}$ excitation pulse with $1\,\text{V}$ amplitude, and the frequency-domain response $H(j\omega)$ defined as the ratio between the received and the transmitted

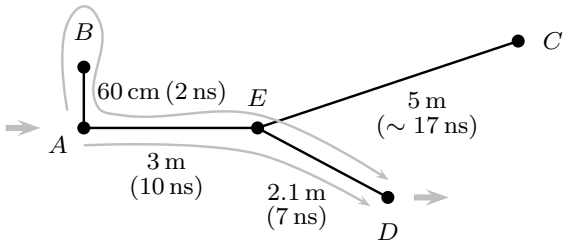

Fig. 4. Power line structure consisting of the interconnection of four transmission lines. As in the previous example, the lines are assumed to be ideal lossless interconnects described by a characteristic impedance $Z_0 = 50\,\Omega$ and suitable length (see the labels in the scheme). The transmitted signal is injected in A via a Thevenin circuit with a $10\,\Omega$ series resistance and observed in D. Three $200\,\Omega$ resistors are placed in B, C and D to terminate the interconnects. The gray lines are two possible paths characterizing the transmission of a signal sent in A and received in D.

voltage signals. The above responses have been obtained via the SPICE simulation of the example structure of Fig. 4. It is worth noticing that the the first two echoes of the transmitted pulse correspond to the gray paths shown in Fig. 4, as highlighted in the top panel of Fig. 5. The starting time of the mentioned echoes can be easily computed from the information of the propagation time along the different lines composing the interconnected structure (see the gray annotations in Fig.s 4 and 5).

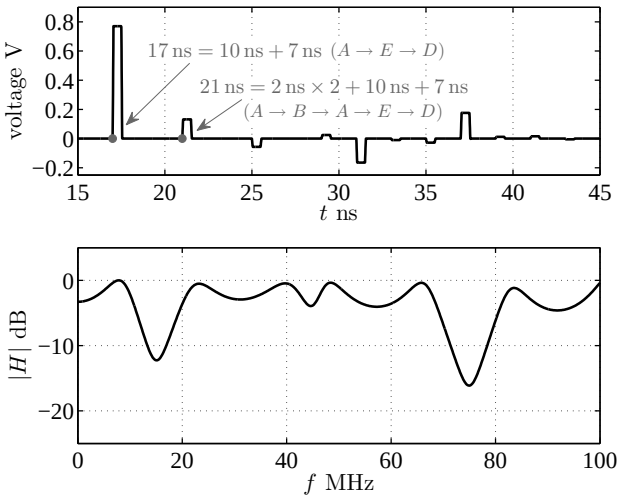

Fig. 5. Time-domain voltage response received at point D of the power line structure of Fig. 4 to a 0.5 ns pulse with unitary amplitude sent in A (top panel). Normalized magnitude of the $H(j\omega)$ transfer function of the example power line computed as the ratio between the received and the transmitted voltages (bottom panel).

This additional example confirms the multipath nature of the four-line interconnected network, that is characterized by a time-domain response consisting of weighted and delayed replicas of the transmitted signal and by a frequency-domain response characterized by a number of local maxima and minima. The above features suggest the typical signature of real power structures that are certainly more complex than the one of Fig. 4 but share the same time- and frequency-domain behavior.

The previous discussion based on the examples of Fig. 1 and Fig. 4 provides a robust and convincing justification of the so-called multipath model representation that has already been successfully used in the literature for the behavioral modeling of a complex power network (e.g. see [29]). The proposed model in the frequency-domain is expressed as:

$$H(j\omega) \approx \sum_{k=1}^{m} g_k \exp(-j\omega\tau_k) \tag{5}$$

where H is a frequency-domain transfer function of interest. In the previous equation, $g_k, k = 1, 2, \ldots$ are the generalization of the weighting coefficients already defined in (2) that account for the attenuation and phase distortion of the transmitted signal. Similarly, the $k-$th exponential term corresponds to the propagation delay τ_k. Clearly, the above equation is a generalization of (2) that can be used to approximate the behavior of an ideal lossless interconnected structure via the sum of a finite number of delay terms. It is relevant to remark that the above model can suitably be modified by including additional frequency dependent weights that account for the cable losses. However, for the specific application at hand and for the frequency range of interest, a simpler lossless form of (5) has been proven to be effectively used.

C. Estimation procedure

This section outlines the proposed procedure for the computation of model parameters from frequency-domain data. Additional details will be provided in Sec. III and Sec. IV where the measurements of a real power line channel are collected and the proposed step-by-step process is applied to the available data, respectively.

The estimation of model (5) is obtained by determining the number of echoes m, the delays τ_k and the linear coefficients g_k. It is important to notice that, for a real structure as the in-vehicle power line, all the previous numbers are unknown parameters depending on either unknown or partially known quantities (such as the geometrical and electrical parameters of the interconnected wires). As an example, the electrical power scheme of a car provides a logical information on the topology of the power networks, without the inclusion of detailed physical information of the structure.

The modeling procedure can be decomposed into the following steps:

Step 1. In this step, the frequency-domain channel responses (as the one of Fig. 2) are collected by means of real measurements carried out on the power line structure (Sec. III provides a detailed discussion of the measurement setup and data acquisition for an automotive application example).

Step 2. Here, the channel impulse response is obtained via the inverse fast Fourier transform (IFFT) of the original frequency-domain data. If the approximation defined by (5) holds, the impulse response turns out to be defined by a number of delayed pulses arising from the exponential terms in the model equation. The position of the pulses along the time axis represents the time delays τ_k. This can be clearly appreciated from the delayed echoes of Fig. 3. Roughly speaking, if the transmitted pulse $e_S(t)$ is narrowed, the different delayed contributions composing the impulse response become thin

ideal peaks located at $t = \tau, 3\tau, 5\tau, \ldots$. Of course, in a real and band-limited measurement of a more complex structure, with many branches and possibly dynamical lumped equivalents terminating the lines, the impulse response turns out to be defined by a set of distorted and possibly overlapping peaks (additional details are given in Sec. IV). Owing to this, all the τ_k determined according to the previous rule values will be included in a set and considered potential delays in the next step.

Step 3. The third step allows to determine the number of delays m, the values $\{\tau_k\}$ selected in the set of potential delays and the linear coefficients $\{g_k\}$. Of course, keeping all the delays found in the first step, would furnish an accurate model. In what follows, however, we want to show that sufficient accuracy can be preserved with a proper selection of them: the possibility to reduce the number of terms m strengthens the value of the multipath model (5). Specifically, this is achieved by considering all the possible M peaks of the impulse response as tentative delays and by recasting the scalar frequency-domain equation (5) in terms of the following linear least squares (LS) problem:

$$\boldsymbol{H} \approx \boldsymbol{D}\boldsymbol{g} \tag{6}$$

where vector $\boldsymbol{H} = [H(j\omega_1), \ldots, H(j\omega_N)]^T$ collects the available tabulated frequency samples known at the N frequencies $\{\omega_1, \ldots, \omega_N\}$[1], matrix $\boldsymbol{D}$ contains the delay terms

$$\boldsymbol{D} = \begin{bmatrix} e^{-j\omega_1\tau_1} & \ldots & e^{-j\omega_1\tau_M} \\ e^{-j\omega_2\tau_1} & \ldots & e^{-j\omega_2\tau_M} \\ \vdots & \vdots & \vdots \\ e^{-j\omega_N\tau_1} & \ldots & e^{-j\omega_N\tau_M} \end{bmatrix} \tag{7}$$

and vector $\boldsymbol{g}$ collects the unknown weighting coefficients $\{g_1, g_2, \ldots, g_M\}$. In order to select the subset of delays leading to the largest reduction of the approximation error, an orthogonal least squares estimation algorithm is used [34]. It provides an effective solution for the inclusion of the dominant m delays in the model by means of an exhaustive search and a forward regression method that can be summarized as follows. The procedure starts with an empty matrix $\boldsymbol{D}$ and each delay in the set is individually considered as a potential contribution to be inserted as the first column of $\boldsymbol{D}$,

$$d_k = [e^{-j\omega_1\tau_k}, e^{-j\omega_2\tau_k}, \ldots, e^{-j\omega_N\tau_k}]^T, \tag{8}$$

$k = 1 \ldots M$. The k-th delay leading to the smallest error is chosen only (e.g. the first column corresponding to τ_1 in (7)). The approximation error is defined by

$$E = \frac{||\boldsymbol{H} - \boldsymbol{D}\boldsymbol{g}||^2}{||\boldsymbol{H}||^2} \tag{9}$$

where $||(\cdot)||$ is the norm assumed in the Euclidean space of complex variables (i.e., $||(\cdot)||^2 =< (\cdot), (\cdot) >= (\cdot)^*(\cdot)$ and the superscript $*$ denoting the Hermitian transpose conjugate operator). Note that E also includes a leakage component due to IFFT/FFT processing.

[1]The superscript T denotes the transpose operator.

The procedure continues with matrix $\boldsymbol{D}$ consisting of one column only and the second column is chosen among the remaining potential delay terms. Again, the contribution leading to the largest error reduction is selected. The procedure iterates with the inclusion of a new column in $\boldsymbol{D}$ at each iteration and terminates at the m-th step when $E < \rho$, where $0 < \rho < 1$ is a chosen tolerance (e.g. $\rho = 0.01$). Once the delay terms are chosen, the $\{g_k\}$ coefficients are determined from the frequency-domain data via the solution of the reduced linear least squares problem in (6). If needed, the model quality can be improved by lowering the error threshold and adding more terms. It is relevant to remark that the proposed solution is an improvement on the algorithm published in [31]. In the latter paper a suboptimal selection is done, all the potential delays are sorted in descending order (i.e. w.r.t. to the magnitude associated to the corresponding peaks of the impulse response) and they are sequentially included in the model until the error (9) is reduced below the threshold. The proposed method has been proven to generate more compact models, i.e. with a smaller number of components, with a reasonable increase of CPU time. Additional results on the comparison between the two advocated algorithms are collected in Sec. V.

It is also worth noticing that the proposed procedure for parameter estimation provides a robust and blind process for the computation of the different model parameters from the observation of frequency-domain responses only. Owing to this, any effort in trying to retrieve all the detailed information on a power line structure does not modify the devised black-box modeling scheme and does not offer major benefits to model accuracy or compactness.

III. Measurements

This study relies on a set of measurements carried out on a popular economy car manufactured by General Motors which has the dimensions and electronic features typical of many compact cars produced by any auto-maker.

Specifically, two-port frequency-domain scattering measurements have been carried out by means of a vector network analyzer (VNA) between different pairs of probing points of the in-vehicle power distribution system. The frequency range is [500 Hz , 100 MHz]: it has been selected with the intention to cover the frequency range of present [15] and future [16] in-home PLC modems. The probing points are the dashboard light and car-radio connectors, on the front side of the console, the trunk and license plate lights and the front and rear lights (indicators, fog lights, reversing lights, dipped headlights, high-beam and parking-light points are considered). For measurements involving the lights as probing points, the associated lamps had to be removed to access the power line: note that in this case the lamps not involved in the measure are in their correct position.

Table I provides a picture that summarizes the measurements carried out in the study and that involve data links defined between different probing points. The rows and the columns of the table correspond to the selected group of probing points and the star symbol corresponds to the data links included in the set. It is relevant to remark that the matrix

of Tab. I is symmetric and its upper triangular portion is filled-in only (gray color is used for the lower triangular part). In addition, a limited number of measurements are considered for links defined by two probing points within the same group (e.g., see the $5-$th, the $6-$th and the $7-$th diagonal entries, for instance the link between the indicator and the parking light inside the same light) with the aim of observing the behavior of adjacent points that do not necessarily exhibit weak attenuation. It is relevant to remark that a detailed analysis of the different grouped measurements is out of the scope of the paper. The aim of the above table was to provide a concise visual picture of the heterogeneous and representative points considered in this assessment to demonstrate the effectiveness of the proposed modeling approach.

TABLE I
SUMMARY OF THE MEASUREMENTS CARRIED OUT ON DIFFERENT PROBING PAIRS OF THE CAR POWER NETWORK.

Groups of probing points $\downarrow \rightarrow$	#1	#2	#3	#4	#5	#6	#7	#8
#1. Trunk light		$*$	$*$	$*$	$*$	$*$	$*$	$*$
#2. Car-radio connector			$*$	$*$	$*$	$*$	$*$	$*$
#3. Dashboard light				$*$	$*$	$*$	$*$	$*$
#4. Front right lights					$*$	$*$	$*$	$*$
#5. Front left lights					$*$	$*$	$*$	$*$
#6. Rear right lights						$*$	$*$	$*$
#7. Rear left lights							$*$	$*$
#8. License plate lights								

During the measurements the car was not running, no gear was inserted and no pedals were pumped (apart for activating the reversing light and the rear parking-lights). Moreover, the electrical systems were generally off (car-radio, windscreen wipers, etc. ...). The following three states of the car have been considered:

- *Key inserted*: in this state all the electrical car equipments are off and the key is inserted in the dashboard rotating plug;
- *Console on, Engine off*: the key is turned (engine ignition does not take place, but some electronic systems like, for instance, the electrical windows and the lights could be used);
- *Engine on*: the motor is in the idle state at 1000 rpm.

The VNA used in this activity is the Agilent E5061B, having a 3 GHz bandwidth and a maximum number of 1601 points/acquisition. In order to make the total number of measured samples as great as possible, the selected VNA allows to automatically serialize up to four different frequency-domain acquisitions in different frequency intervals. Based on the above feature, the measurements have been done by subdividing the whole frequency range into the following bands: $[0.5, 800]$ kHz, $[800, 1600]$ kHz, $[1.6, 51]$ MHz and $[51, 100]$ MHz. Of course, four 2-port calibrations were required and carried out before performing the measurements.

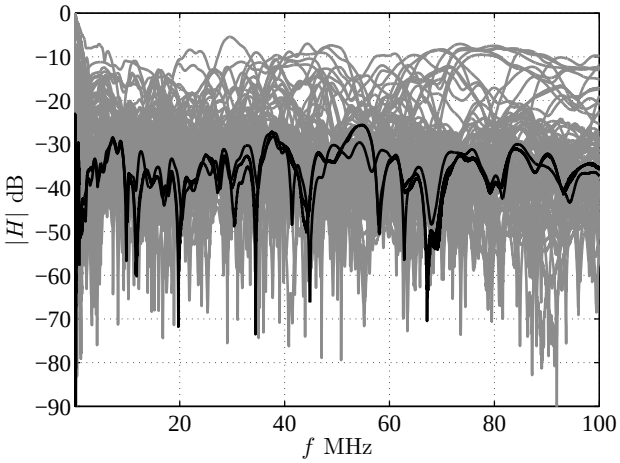

Fig. 6. Magnitude of the power line channel network function $H(j\omega)$ of the test vehicle. The frequency range is [500 Hz , 100 MHz]. The gray curves belong to the complete set of 106 measurements corresponding to different links and/or possible operating states of the car. The black thick lines are the measurements associated with the link between the front left headlight and the power-supply connector of the car-radio, for the three different operating states.

As an example, Fig. 6 shows the magnitude of the S_{21} scattering parameter associated with all the 106 measured links and/or operating states considered. The scattering parameter $S_{21}(j\omega)$ is the network function $H(j\omega)$ describing the wave transmission between port 1 and port 2 of the instrument (e.g., see [33] for a self-contained presentation of scattering parameters). The black curves of Fig. 6 are the responses associated with the link between the front left headlight and the power-supply connector of the car-radio, recorded during the three different operating states of the car. The latter responses, which exhibit the typical signature of frequency-domain responses of the in-vehicle power structure, will be considered in Sec. IV for illustrating the proposed step-by-step modeling procedure. Of course, once the procedure is defined and tuned based on a limited selection of curves, it will be systematically applied to all the other measurements in order to verify the feasibility and robustness of the modeling method for the specific application at hand (see Sec. V).

For a given link, the measurements of the two-port scattering parameters have been carried out according to the ideal setup of Fig. 7. The scheme of Fig. 7 highlights two blocks (labeled as DC1 and DC2 in the figure) that consist of the cascade connection of a DC block and of a probe tip. The DC block and the probe tip protect the VNA and connect the instrument output coaxial cable to the test points of the car electrical network, respectively. Based on the setup of Fig. 7, the effects of the two blocks DC1 and DC2 on the channel measurement can be effectively de-embedded via the following strategy. The original data are the measured scattering parameters between port 1 and port 4. These data can be suitably interpreted as the responses of a cascaded connection of the three blocks of Fig. 7. Hence, by using the scattering transfer representation, the cascade of Fig. 7 is represented by the following expression

$$\begin{bmatrix} A_1 \\ B_1 \end{bmatrix} = \underbrace{\boldsymbol{U}_{\mathrm{DC1}}\boldsymbol{U}_{\mathrm{channel}}\boldsymbol{U}_{\mathrm{DC2}}}_{\boldsymbol{U}_{\mathrm{meas}}} \begin{bmatrix} A_4 \\ B_4 \end{bmatrix} \tag{10}$$

where $A_k = (V_k + Z_0 I_k)/2$ and $B_k = (V_k - Z_0 I_k)/2$, $k = 1, 4$ are the incident and the reflected voltage waves associated to the left-hand and right-hand ports of the cascaded structure, respectively, and Z_0 is the reference impedance assumed for the scattering representation ($Z_0 = 50\,\Omega$ in this case). From (10) it is clear that the characteristic of the channel can be obtained from the information on the characteristics of the test fixture, i.e. from $\boldsymbol{U}_{\mathrm{DC1}}$ and $\boldsymbol{U}_{\mathrm{DC2}}$:

$$\boldsymbol{U}_{\mathrm{channel}} = \boldsymbol{U}_{\mathrm{DC1}}^{-1}\boldsymbol{U}_{\mathrm{meas}}\boldsymbol{U}_{\mathrm{DC2}}^{-1} \tag{11}$$

The scattering parameters of the blocks DC1 and DC2 are obtained by means of a separate VNA characterization of the blocks.

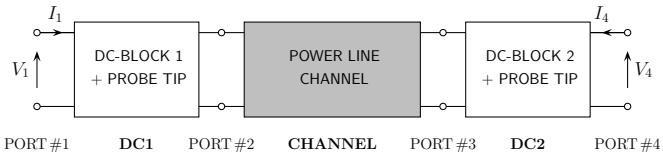

Fig. 7. Ideal setup for the frequency-domain measurements of a power line communication channel by means of a VNA. Complex electrical voltage and current variables are shown in the scheme.

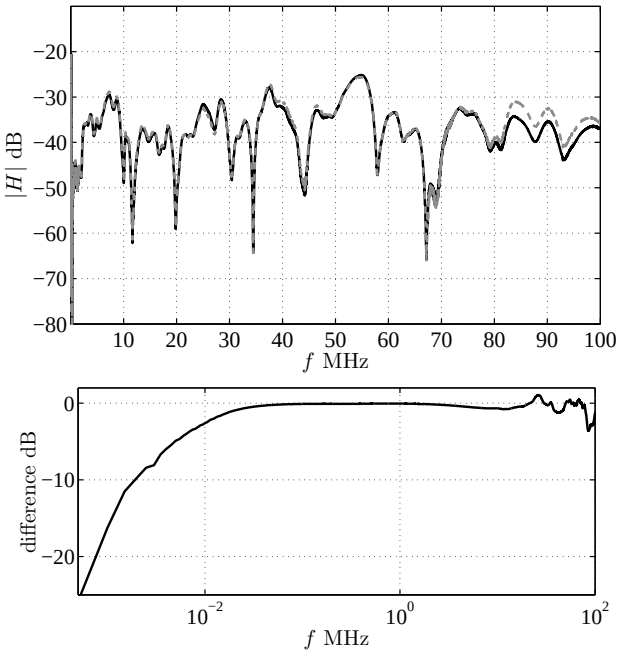

Fig. 8. Top panel: magnitude of $H(j\omega)$ of the selected black curve of Fig. 6. The two curves are the measured response (black line) and the response obtained via the de-embedding process (dashed gray line). Bottom panel: difference between the two curves in the subplot on top. A logarithmic scale is used for the $f-$axis to highlight the effects of the DC bias blocks that unavoidably lead to larger differences in the low frequency region.

Fig. 8 shows the magnitude of $H(j\omega)$ corresponding to one of the black curves of Fig. 7. The two responses in Fig. 8, which are the measured parameter and the parameter obtained from (11), clearly highlight the effects of the test fixture on the frequency-domain behavior of the power line channel. It is relevant to remark that all the curves shown in Fig. 6 have been processed by applying the above procedure.

IV. Numerical results

In this section, the modeling procedure outlined in Sec. II-C is applied to the real measurements of Fig. 6 (i.e. see **step 1**). A grid of uniformly sampled frequency points is considered for the collection of the tabulated data feeding the different estimation steps. All the results collected in this study have been obtained with a sampling interval $f_s = 300\,\mathrm{kHz}$.

According to **step 2**, the impulse response of the channel is computed via the IFFT of the original frequency-domain data. Note that the position of the pulses along the time axis represents the time delays τ_k. As an example, the black curve of Fig. 9 is the impulse response arising from the processing of $H(j\omega)$ corresponding to one of the black curves of Fig. 6. The time-domain response has been obtained by means of the MATLAB® function `ifft.m`. It is worth noting that the typical bandwidth of the measurements for this class of applications, which is on the order of one hundred MHz, leads to an impulse response with a low timing resolution that hardly allows the estimation of the position of the peaks. Owing to this, the resolution of the impulse response needs to be improved via standard techniques such as zero-padding that amounts to appending zeros to the frequency-domain response up to a larger frequency. The effect of zero-padding can be appreciated from the gray curve of Fig. 9 that represents the same impulse response generated by filling in the selected frequency-domain response with zeros up to a maximum frequency of $500\,\mathrm{MHz}$. Clearly, zero-padding does not introduce additional information and also highlights the possible spurious oscillations coming from the IFFT of a signal that has a limited bandwidth. However, it allows to easily locate the sharp pulses composing the impulse response and therefore the set of potential delays that will be possibly included in model (5).

In **step 3**, the model parameters, i.e. a selection of the $\{\tau_k\}$ delays, their number m and the corresponding linear coefficients $\{g_k\}$ are computed from the curve of Fig. 6 according to the detailed procedure. For the example at hand, only the delays corresponding to the circles in Fig. 10 leading to an error E below 1×10^{-2} are selected. The total number of selected delays is $m = 56$. Fig. 11 compares the measured frequency-domain transfer function of the selected $H(j\omega)$ to the prediction obtained by means of (5), thus highlighting that a relatively limited number of terms leads to a compact and accurate model that can be effectively used to reproduce the behavior of the PLC channel. Similar results can be obtained for different links. In addition, Tab. II shows the figures of the model complexity and accuracy for different values of the approximation error chosen during the selection of the delays (see the previous step). The complexity is quantified by the number of delays included in the model and the accuracy

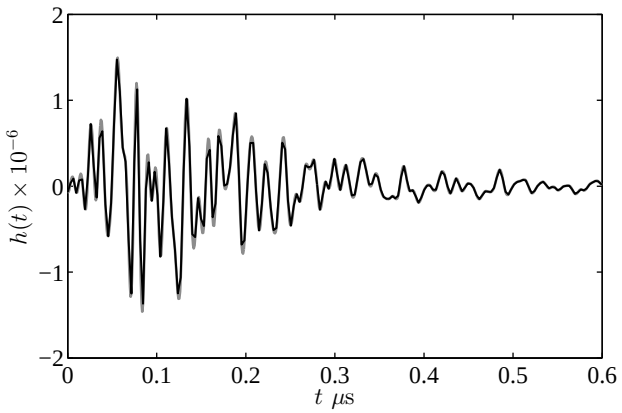

Fig. 9. Impulse response obtained via the inverse FFT of the selected $H(j\omega)$. Black curve: direct application of the `ifft` MATLAB function; Gray curve: response with increased time-resolution obtained by zero-padding the original frequency-domain response up to 500 MHz.

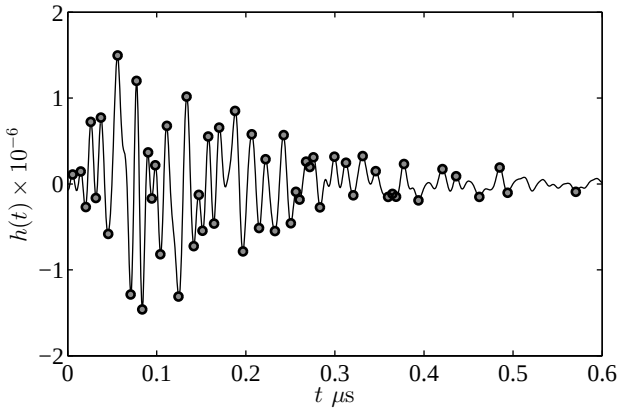

Fig. 10. Automatically selected peaks of the impulse response of Fig. 9 (see the circles superimposed to the impulse response). The abscissas of the selected peaks are the delay parameters of model (5).

by means of the error in (9) computed from the sampled frequency-domain responses of Fig. 11.

For a specific data link, the variability of the channel responses can be possibly added to the model equations. For a specific data link, the variability is due to the operating states of the car and the electronic apparatus connected to the power distribution. The number and values of the delays are assumed to be constant since the physical lengths of the wires and the network topology do not change, and the variability is included in the weighting coefficients g_k of (5) instead. This means that in the problem defined by (6), matrix $\boldsymbol{D}$ is filled with the columns associated to the selected delays only. Hence, from

TABLE II
FIGURES OF THE MODEL COMPLEXITY AND ACCURACY FOR DIFFERENT VALUES OF THE RELATIVE THRESHOLD ADOPTED DURING THE AUTOMATIC SELECTION OF THE DELAYS.

E	0.1	5e-2	2e-2	**1e-2**	5e-3	1e-3	5e-4
m	21	28	46	**56**	63	94	108

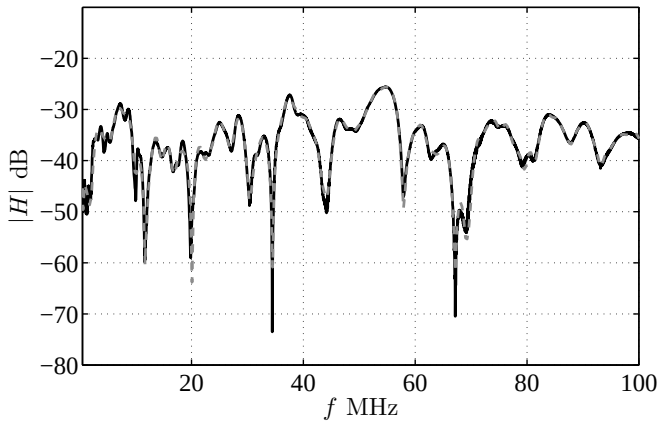

Fig. 11. Magnitude of the $H(j\omega)$ reference network response. Solid black: measurement; dashed gray: model response.

measurements of the same link in different conditions, the g_k unknowns corresponding to the different operating states are computed via simple linear inversion of (6).

A set of deterministic linear coefficients has been computed from the black curves of Fig. 6 besides the one used in Fig. 11, via the solution of the same reduced least squares problem (6). In this computation, the set of delays $\{\tau_k\}$ are those computed in the previous step. As an example, Fig. 12 shows the same comparison of Fig. 11 for different operating states. This comparison further confirms the accuracy of the proposed model and of the presented modeling procedure. In order to gain insight into the variability of model parameters, Fig. 13 shows the magnitude of the linear weighting coefficients g_k associated with the selected delays of Fig. 10. For each delay in the abscissa, the different symbols represent the $k-$th coefficient computed from the set of three responses of the same link under study.

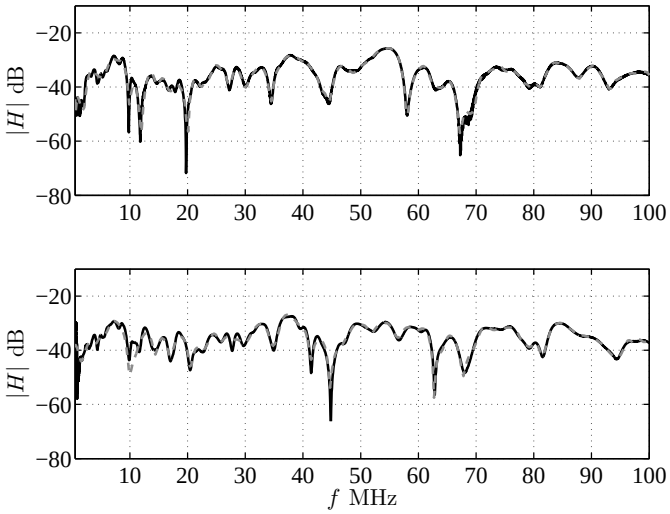

Fig. 12. Magnitude of the $H(j\omega)$ of a selection of two alternative measurements. Solid black: measurements; dashed gray: model responses.

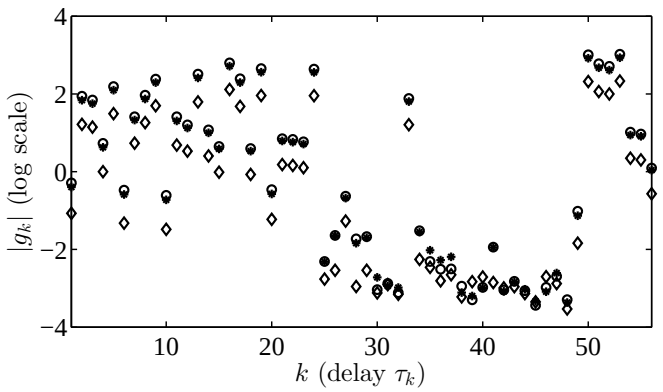

Fig. 13. Linear coefficients g_k of (5). Circles, dots and diamonds are used to identify the set of coefficients associated to three different operating states of the car (see Sec. III for details).

V. Statistical assessment

This section collects the results of the application of the proposed technique and of the method presented in [31] to all the measurements carried out on the test vehicle during this study. The aim of this systematic assessment is to collect some useful statistical information on the model complexity, i.e. on the number of delay terms required for a predefined model accuracy and for a large possible variety of links occurring in an automotive PLC channel. The CPU time required by the different algorithms is reported as well.

Tables III and IV summarize the results of this additional test, where the information on the percentile of the number of model delays m is given. The values in the tables were obtained for a model quality defined by (9) and two different values of the error E. As an example, the third row of Tab. III highlights that fifty percent of the links can be approximated by models with an error E lower than 1×10^{-2} and with a number of terms lower than 75. Similarly, if the model accuracy is reduced to $E = 5 \times 10^{-2}$, the behavior of a larger number of links (ninety percent) can be approximated by models with less than 69 terms.

It is also worth noting that, in practice, model accuracies even larger than the ones considered in Tab. III are sufficient to generate models that are able to capture the dominant frequency-domain behavior of PLC channels. In the latter case, the complexity of the models is extremely low, thus facilitating the storage and the processing of the model coefficients in a hardware or software channel emulator. Also, the numbers in the tables clearly highlight that the proposed estimation algorithm allows to generate more compact models, i.e. models with less delay terms for the same predefined accuracy.

Table V concludes the comparison with the average CPU time required to run the two alternative estimation algorithms on a single frequency-domain measurement. The information in Tab. V is computed from the processing of the complete set of 106 measurements. As already outlined in the previous section, the proposed algorithm guarantees less delay terms in the model with an unavoidable increase of the estimation time due to a stepwise exhaustive search of the best components. However, the CPU time is still affordable and does not prevent the application of the method to real measured data. It is relevant to remark that the algorithm for parameter estimation is run only once, thus allowing researchers to use the synthetic channel descriptions imitating the behavior of the real power line structures for the assessment of different design scenarios. Owing to this, a possible overhead in the initial phase of the activity turns out to be negligible. Summarizing, once the model parameters are computed (i.e., the coefficients g_k and the delays τ_k of (5) are determined) the channel is described by means of a simple mathematical equation with a limited number of coefficients.

TABLE III
Statistics of the number of delays obtained by applying the proposed technique to the 106 measurements of Fig. 6 (improved algorithm proposed in Sec. II-C).

	m ($E \leq 0.01$)	m ($E \leq 0.05$)
Average	85	40
1–st quartile (25%)	49	24
Median (50%)	75	35
3–rd quartile (75%)	96	50
90–th percentile (90%)	129	69

TABLE IV
Statistics of the number of delays obtained by applying the proposed technique to the 106 measurements of Fig. 6 (algorithm [31]).

	m ($E \leq 0.01$)	m ($E \leq 0.05$)
Average	98	48
1–st quartile (25%)	55	26
Median (50%)	89	40
3–rd quartile (75%)	117	59
90–th percentile (90%)	155	87

TABLE V
Average CPU time required for model generation with the two alternative estimation algorithms considered in this study.

Algorithm	$E \leq 0.01$	$E \leq 0.05$
[31]	0.15 s	0.12 s
proposed	2.2 min	13 s

VI. Conclusions

In this paper, a behavioral approach for the experimental modeling of a power distribution network is presented.

The model assumed to reproduce the behavior of a generic power line channel is a parametric representation describing the multipath transmission of signals on a possibly complex interconnected structure. Model parameters, that consist of a set of weighting coefficients associated to ideal delay terms, are estimated from frequency-domain data via a well defined step-by-step procedure. An automotive power line channel measurement campaign is presented as well. The channel between several probing points of a commercial automobile has been measured within different operating states of the car. Moreover, the effect of de-embedding on the measured responses is thoroughly discussed. The proposed modeling technique is systematically applied to all the available measurements to verify the strength of the model and to collect some statistical information useful to drawn conclusions holding for the specific application at hand.

ACKNOWLEDGMENT

Luca Rigazio, Goma Elettronica S.p.A., Torino, Italy (formerly Politecnico di Torino, Italy), is acknowledged for his valuable support during the measurement activities. The authors wish to express their gratitude to Roberto Cappelletti, Maria Rosa Borghi, Pietro Menniti and Roberto Gariboldi for continuing support during this work.

REFERENCES

[1] N. Navet, Y. Song, F. Simonot-Lion and C. Wilvert, "Trends in Automotive Communication Systems," *IEEE Proceedings*, Vol. 93, No. 6, pp. 1204–1223, June 2005.

[2] T. Nolte, H. Hansson and L. Lo Bello, "Automotive Communications - Past, Current and Future," Proc. of the *IEEE Conference on Emerging Technologies and Factory Automation (ETFA),* Vol. 1, Catania, Italy, pp. 992–999, 19–22 September 2005.

[3] G. Leen and D. Heffernan, "Expanding Automotive Electronic Systems," *IEEE Computer*, Vol. 35, No. 1, pp. 88-93, January 2002.

[4] F. Benzi, T. Facchinetti, T. Nolte and L. Almeida, "Towards the Powerline Alternative in Automotive Applications," Proc. of the *IEEE Int. Workshop on Factory Communication Systems (WFCS)*, Dresden, Germany, pp. 259-262, 21–23 May 2008.

[5] T. Sauter and M. Lobashov, "End-to-End Communication Architecture for Smart Grids," *IEEE Transactions on Industrial Electronics*, Vol. 58, No. 4, pp. 1218–1228, April 2011.

[6] N. Pavlidou, A. J. Han Vinck, J. Yazdani and B. Honary, "Power Line Communications: State of the Art and Future Trends," *IEEE Comm. Magazine*, Vol. 41, No. 4, pp. 34–40, April 2003.

[7] W. Stefanutti, S. Saggini, P. Mattavelli and M. Ghioni, "Power Line Communication in Digitally Controlled DC–DC Converters Using Switching Frequency Modulation," *IEEE Trans. on Industrial Electronics*, Vol. 55, No 4, pp. 1509–1518, April 2008.

[8] B. Vallbe, J. Balcells, P. Bogonez-Franco, J. Mata and X. Gago, "Immunity of Power Line communications (PLC) in Disturbed Networks," Proc. of the *2011 IEEE Int. Symp. on Industrial Electronics (ISIE)*, Gdansk, Poland, pp. 1621–1625, 27–30 June 2011.

[9] E. Roman, R. Alonso, P. Ibanez, S. Elorduizapatarietxe and D. Goitia, "Intelligent PV Module for Grid-Connected PV Systems," *IEEE Trans. on Industrial Electronics*, Vol. 53, No. 4, pp. 1066–1073, June 2006.

[10] G. Acciani, V. Amoruso, G. Fornarelli and A. Giaquinto, "Numerical Analysis of Synchronous Impulsive Noise on Naval Powerline communications," Proc. of the *2010 IEEE Int. Symp. on Industrial Electronics (ISIE)*, Bari, Italy, pp. 2973–2978, 4–7 July 2010.

[11] O. G. Hooijen, "A Channel Model for the Residential Power Circuit used as a Digital Communications Medium," *IEEE Transactions on Electromagnetic Compatibility*, Vol. 40, No. 4, pp. 331–336, November 1998.

[12] T. Dragičević, J. M. Guerrero and J. C. Vasquez, "A Distributed Control Strategy for Coordination of an Autonomous LVDC Microgrid Based on Power-Line Signalling," *IEEE Trans. on Industrial Electronics*. 2014 (accepted, in press).

[13] C. P. Rui, N.N. Barsoum, A.W-K. Ming and W. K. Ing, "Adaptive Impedance Matching Network with Digital Capacitor in Narrowband Power Line Communication," Proc. of the *2013 IEEE Int. Symp. on Industrial Electronics (ISIE)*, Taipei, Taiwan, pp. 1–5, 28–31 May 2013.

[14] Chung-Chuan Hou and Yu-Chun Chen, "A Hybrid Islanding Detection for Distributed Generation Systems using Pulse Current Injection", Proc. of the *IEEE Int. Symp. on Industrial Electronics (ISIE)*, Hangzhou, China, pp. 1554–1559, 28–31 May 2012.

[15] HomePlug Alliance, "HomePlug AV White Paper" (available online @ http://www.homeplug.org).

[16] HomePlug Alliance, "HomePlug AV specification," v. 2.0, Jan. 2012 (available online @ http://www.homeplug.org).

[17] S. Kelkar and R. Rajkamal, "Control Area Network Based Quotient Remainder Compression-Algorithm for Automotive Applications", Proc. of the *38th Annual Conference on IEEE Industrial Electronics Society (IECON)*, Montreal, QC, pp. 3030–3036, 25–28 October 2012.

[18] N. Taherinejad, R. Rosales and L. Lampe, "Channel Characterization for Power Line Communication in a Hybrid Electric Vehicle," Proc. of the *2012 IEEE Int. Symp. on Power Line Communications and its Applications (ISPLC)*, Beijing, China, pp. 328–333, 27–30 March 2012.

[19] A. B. Vallejo-Mora, J. J. Sánchez-Martínez, F. J. Canéte and J. A. Cortés, L. Díez, "Characterization and Evaluation of In-Vehicle Power Line Channels," Proc. of the *53–th Annual IEEE Global Telecommunications Conference (GLOBECOM)*, Miami, FL, pp. 1–5, 6–10 December 2010.

[20] M. Lienard, M.O. Carrion, V. Degardin and P. Degauque, "Modeling and Analysis of In-Vehicle Power Line Communication Channels," *IEEE Trans. on Vehicular Technology,* Vol. 57, No. 2, pp. 670–679, March 2008.

[21] L.T. Berger and G. Moreno-Rodriguez, "Power Line Communication Channel Modeling through Concatenated IIR-Filter Elements," *Journal of Communications,* Vol. 4, No. 1, pp. 41–51, February 2009.

[22] T. Esmailian, F. R. Kschischang and P. G. Gulak, "In-Building Power Lines as High-Speed Communication Channels: Channel Characterization and a Test Channel Ensemble," *Int. Journal of communication systems*, Vol. 16, No. 5, pp. 381–400, June 2003.

[23] T. Esmailian, F. R. Kschischang and P. G. Gulak, "An In-Building Power Line Channel Simulator," Proc. of the *2002 Int. Symp. on Power Line Communications and its Applications (ISPLC)*, Athens, Greece, pp. 31–35, March 2002.

[24] S. Barmada, M. Raugi, M. Tucci and T. Zheng, "Power Line Communication in a Full Electric Vehicle: Measurements, modelling and analysis," Proc. of the *2010 IEEE Int. Symp. on Power Line Communications and Its Applications, (ISPLC)*, Rio de Janeiro, Brazil, pp. 331–336, 28–31 March 2010.

[25] T. Zheng, M. Raugi and M. Tucci, "Analysis of Transmission Properties of Naval Power Line Channels," Proc. of the *2010 IEEE Int. Symp. on Industrial Electronics (ISIE)*, pp. 2955–2960, 4–7 July 2010.

[26] J. Proakis, *Digital Communications*, 3-rd ed. New York, McGrawHill, 1995.

[27] M. Mohammadi, et. Al., "Measurement Study and Transmission for In-Vehicle Power Line Communication," Proc. of *2009 IEEE Int. Symposium on Power Line Communications and Its Applications, ISPLC*, Dresden, Germany, pp. 73–78, Mar. 29 – 1 April 2009.

[28] W. Gouret, F. Nouvel and G. El-Zein, "Additional Network Using Automotive Powerline Communication," Proc. of *6-th Int. Conference on ITS Telecommunications,* Chengdu, China, pp. 1087–1089, June 2006.

[29] M. Zimmermann and K. Dostert, "A Multipath Model for the Powerline Channel," *IEEE Trans. on Communications*, Vol. 50, No. 4, pp. 553–559, April 2002.

[30] I.S. Stievano, F.G. Canavero and V. Dafinescu, "Power Line Communication Channel Modeling for In-Vehicle Applications," Proc. of the *2012 IEEE Int. Instrumentation and Measurement Technology Conference (I2MTC)*, Graz, Austria, pp. 376–379, 13–16 May 2012.

[31] I.S. Stievano and F.G. Canavero, "Behavioral Modeling of Power Line Communication Channels for Automotive Applications," Proc. of the *16−th IEEE Int. Symp. on Power Line Communications and its Applications (ISPLC 2012)*, Beijing, China, pp. 340–343, 27–30 March 2012.

[32] C. R. Paul, "Analysis of Multiconductor Transmission Lines," Wiley, 1994.

[33] I.A. Maio, "A Primer on Scattering Parameters, Part I: Definitions and Properties," *IEEE EMC Society Newsletter*, No. 217, pp. 57–63, Spring 2008.

[34] S. Chen, C. F. N. Cowan and P. N. Grant, "Orthogonal Least Squares Learning Algorithm For Radial Basis Function Networks," *IEEE Trans. on Neural Networks*, Vol. 2 , No. 2, pp. 302–309, March 1991.

Igor S. Stievano (M'98–SM'08) received the master's degree and the PhD degree in electronic engineering from the Politecnico di Torino, Torino, Italy, in 1996 and in 2001, respectively. Currently he is an Associate Professor of Circuit Theory with the Department of Electronics and Telecommunications, Politecnico di Torino. His research interests are in the field of Electromagnetic Compatibility and Signal Integrity, where he works on the macromodeling of linear and nonlinear circuit elements, with specific focus on the behavioral modeling of digital integrated circuits, transmission lines and linear junctions and on the development of stochastic models for the inclusion of uncertainties. He is Author of more than 100 papers published in international journals and conference proceedings. He served as a reviewer for several IEEE journals and in the period 2007–2011 he has been member of the Scientific Steering Committee of the IEEE Int. Workshop on Electromagnetic Compatibility of Integrated Circuits, EMC Compo.

Flavio G. Canavero (SM '99, F '07) received his electronic engineering degree from Politecnico di Torino (Technical University of Turin, Italy) and the PhD degree from the Georgia Institute of Technology, Atlanta, USA, in 1986. Currently he is a Professor of Circuit Theory and Electromagnetic Compatibility with the Department of Electronics and Telecommunications, Politecnico di Torino, where he serves also as the Director of the Doctoral School. He is an IEEE Fellow, Associate Editor of the Letter Section of the IEEE Transactions on Electromagnetic Compatibility, and V.P. for Communication Services of the EMC Society. He has been the Editor-in-Chief of IEEE Transactions on Electromagnetic Compatibility, and Chair of URSI Commission E (Noise and Interference). He received the International Business Machines Corporation (IBM) Faculty Award for the triennium 2003–2005, the Intel Research Grant for 2008, and several Best Paper Awards and IEEE recognitions. His research interests include Signal Integrity and EMC design issues, interconnect modelling, black-box characterization of digital integrated circuits, EMI and Statistics in EMC.

Williams Richard Garcia Valverde received the Masters degree in electronics engineering from the Politecnico di Torino, Turin, Italy in 2004. In 2005 he reached DORA S.p.A. (STMicroelectronics group). He was engaged in the modeling and design of the interface between the DSP and analog front end of the new generation of the narrow band power line modems of STMicroelectronics. He was involved in the validation, verification, prototyping and debug of the newest STMicroelectronics PLC SoCs.

Lorenzo Guerrieri received the master degree (summa cum laude) in Mathematics from the University of Bologna, Italy, in 2002. In the same year, he joined DORA S.p.A., today a company of STMicroelectronics Group, in Aosta, Italy. Here he developed driving algorithms for nematic and bistable liquid crystal display. Since the last few months of 2004, he has been working on power line communications, on the research, development and standardization of narrow and wideband modems for metering and in-home applications. In mid-2010, he became member of STMicroelectronics Technical Staff. Since May 2011, he is member of the SC 210A/ITE committee of the Italian Electrotechnical Committee, appointed to CENELEC TC 210 WG11 from June 2013.

Paola Bisaglia received the Master's degree in electronic engineering and the Ph.D. degree in telecommunication engineering from the University of Padova, in 1996 and 2000, respectively. In 2000 she joined Hewlett-Packard Research Laboratories in Bristol, England, where she worked on home phone-line networking and wireless local area networks. From 2002 to 2005 she was a research fellow at the Department of Information Engineering of the University of Padova, investigating pre and post-detection strategies for next generation (4G) broadband cellular systems. She has been with DORA S.p.A., a company of STMicroelectronics Group, since May 2005, where she is involved in research activities and in the design of integrated circuits for narrow-band and wide-band power-line communications dedicated to indoor and access applications. In July 2010 she became a senior member of the Technical Staff of STMicroelectronics.